Key Points:
- SW2 minimum occurs at middle-high latitudes in the Northern Hemisphere mesosphere-lower thermosphere (80–110 km) around September equinox
- The minimum is related to seasonal transition of the mean zonal winds in the middle atmosphere and their influence on different Hough modes
- Interannual variability in the timing of the SW2 minimum is related to timing of the seasonal transition in middle atmosphere zonal winds

Correspondence to:
N. M. Pedatella,
nickp@ucar.edu

Migrating Semidiurnal Tide During the September Equinox Transition in the Northern Hemisphere

N. M. Pedatella[1,2] [ID]**, H.-L. Liu[1]** [ID]**, J. F. Conte[3]** [ID]**, J. L. Chau[3]** [ID]**, C. Hall[4]** [ID]**, C. Jacobi[5]** [ID]**, N. Mitchell[6,7], and M. Tsutsumi[8]** [ID]

[1]High Altitude Observatory, National Center for Atmospheric Research, Boulder, CO, USA, [2]COSMIC Program Office, University Center for Atmospheric Research, Boulder, CO, USA, [3]Leibniz Institute of Atmospheric Physics, Rostock University, Kühlungsborn, Germany, [4]Tromsø Geophysical Observatory, The Arctic University of Norway, Tromsø, Norway, [5]Institute for Meteorology, Universität Leipzig, Leipzig, Germany, [6]Department of Electronic and Electrical Engineering, University of Bath, Bath, UK, [7]British Antarctic Survey, Cambridge, UK, [8]National Institute of Polar Research, Tokyo, Japan

Abstract Specified Dynamics Whole Atmosphere Community Climate Model with thermosphere-ionosphere eXtension simulations are used to investigate the solar migrating semidiurnal tide (SW2) around September equinox at middle to high latitudes in the Northern Hemisphere. A pronounced minimum in SW2 occurs around September equinox, and is characterized by a ~50% reduction in tidal amplitudes for 20–30 days. Analysis of the simulation results indicates that the SW2 minimum occurs due to the seasonal transition of the zonal mean zonal winds, which alter the generation and propagation of different symmetric and antisymmetric modes of SW2. In particular, the antisymmetric modes notably decrease due to the more hemispherically symmetric zonal winds around equinox. It is further demonstrated that interannual variability in the timing of the SW2 minimum is related to the timing of the seasonal transition of the zonal mean zonal winds in the middle atmosphere. This leads to an earlier occurrence of the SW2 minimum during years when the seasonal transition occurs earlier, such as the recent 2019 September equinox which saw an earlier transition of the Southern Hemisphere zonal mean zonal winds following the occurrence of a sudden stratosphere warming. The connection between the timing of the SW2 minimum in the Northern Hemisphere and the timing of the seasonal transition in the middle atmosphere winds is confirmed by seasonal variability of 12-h tides deduced from specular meteor radar observations at middle to high latitudes in the Northern Hemisphere.

1. Introduction

Solar driven atmospheric tides are forced by the absorption of solar radiation by water vapor and ozone, as well as latent heat release by deep convection. Though generated in the troposphere and stratosphere, atmospheric tides achieve large amplitudes at mesosphere and lower thermosphere (MLT) altitudes, and significantly influence the middle and upper atmosphere. Their impacts include modulating the propagation of gravity waves (Eckermann & Marks, 1996; Fritts & Vincent, 1987; H.-L. Liu & Hagan, 1998; Senf & Achatz, 2011), altering the MLT circulation and chemistry (Akmaev & Shved, 1980; Forbes et al., 1993; Jones Jr. et al., 2014; Miyahara & Wu, 1989; Pedatella et al., 2016; Yamazaki & Richmond, 2013) as well as impacting the electrodynamics of the ionosphere (Fesen et al., 2000; H.-L. Liu & Richmond, 2013; Millward et al., 2001). Atmospheric tides thus play a key role in coupling different regions of the atmosphere, making it critical to understand their variability on different time scales. Tidal variability occurs due to changes in the tidal forcing in the troposphere-stratosphere (Lieberman et al., 2007; Siddiqui et al., 2019; Warner & Oberheide, 2014), changes in the mean winds (Lindzen & Hong, 1974; Stening et al., 1997), and non-linear tide-tide and tide-planetary wave interactions (Angelats i Coll & Forbes, 2002; He et al., 2017; Palo et al., 2007; Teitelbaum & Vial, 1991).

The zonal mean zonal winds that impact tidal propagation exhibit distinct seasonal variations. At middle to high latitudes in the stratosphere and MLT, the seasonal variability is due to variations in solar heating and gravity waves (Andrews et al., 1987). In the middle to high latitude stratosphere and mesosphere, the zonal mean zonal winds are eastward during winter and westward during summer, with opposite directed winds at higher altitudes (Jacobi et al., 2009; Swinbank & Ortland, 2003). Around equinox, the zonal mean
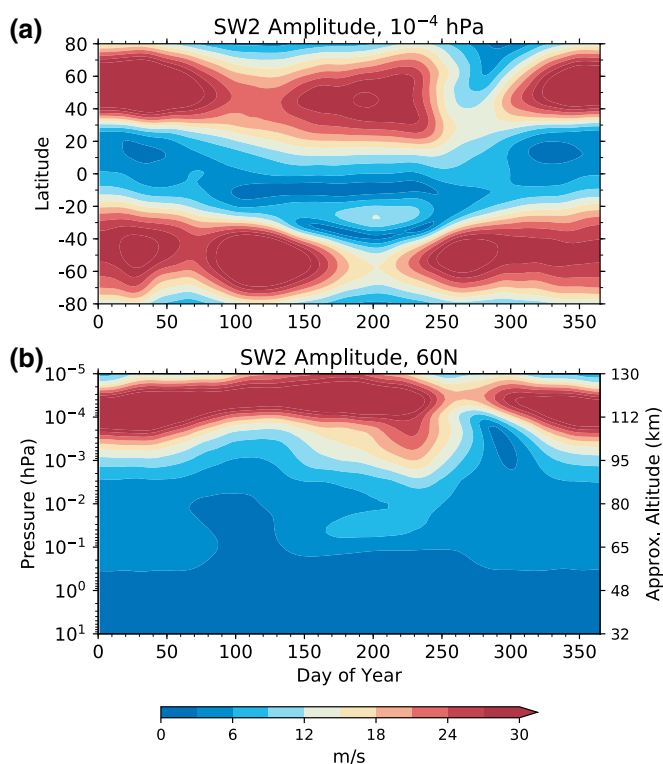
Figure 1. SD-WACCMX climatological SW2 amplitude in zonal wind at (a) 10^{-4} hPa ($\sim$112 km), and (b) 60°N. Results are based on the 1980–2016 average. SD-WACCMX, Specified Dynamics Whole Atmosphere Community Climate Model with thermosphere-ionosphere eXtension.

zonal winds are nearly zero during the transition from summer to winter, or winter to summer. The weak zonal mean zonal winds that occur throughout the middle atmosphere around equinox significantly impact wave propagation, leading to enhanced planetary wave and tidal variability (Lieberman et al., 2003; H.-L. Liu et al., 2001, 2004, 2007; Talaat et al., 2001; Taylor et al., 2001). It is important to note that the timing of the equinox transition in the stratosphere is variable, and can depend on wave forcing as well as ozone concentrations (McLandress et al., 2010; Waugh et al., 1999; Waugh & Randel, 1999). Changes in the timing of the seasonal transition in the stratosphere can further impact the timing of the equinox transition in the mesosphere (Smith et al., 2010; Venkateswara Rao et al., 2015). Although the seasonal transition of the middle atmosphere winds does not always occur during March or September, throughout the following we will use the terminology of September equinox to refer to the seasonal transition between summer and winter in the Northern Hemisphere (winter and summer in the Southern Hemisphere) despite the fact that this transition does not always occur during September. Variability in the winter stratosphere is also known to be a source of variability in the summer mesosphere (Körnich & Becker, 2010; Smith et al., 2020).

The present study focuses on the role of the seasonal transition of the zonal mean zonal winds around September equinox on the migrating semidiurnal solar tide (SW2). The SW2 is primarily forced by the absorption of solar ultraviolet radiation in the stratosphere, and its propagation into the MLT is significantly impacted by the zonal mean zonal winds (Hagan et al., 1992; Hong & Lindzen, 1976; Jin et al., 2012). Previous studies (Chau et al., 2015; Conte et al., 2018) have shown that a deep minimum occurs in the SW2 around September equinox at middle to high latitudes in the Northern Hemisphere. This feature is illustrated in Figure 1, which shows the 1980–2016 climatological amplitude of SW2 at 10^{-4} hPa (Figure 1a) and at 60°N (Figure 1b) from Specified Dynamics Whole Atmosphere Community Climate Model with thermosphere-ionosphere eXtension (SD-WACCMX) simulations. From Figure 1 it is apparent that the SW2 amplitude at middle to high latitudes in the Northern Hemisphere has a deep minimum around September equinox. The minimum lasts for $\sim$20–30 days, and is characterized by an amplitude reduction in excess of 50%. Though clearly identified in both model simulations and observations, the source of the pronounced SW2 minimum in the Northern Hemisphere around September equinox remains unknown. SW2 minima around the March equinox are also apparent in both hemispheres in Figure 1; however, these are not as deep and pronounced as the Northern Hemisphere minimum that occurs around the September equinox. We thus focus the present study on the latter.

The objective of the present study is to investigate the source of the SW2 climatological minimum that occurs at middle to high latitudes in the Northern Hemisphere around September equinox. Motivated in part by the early seasonal transition in the Southern Hemisphere stratosphere following the recent 2019 Southern Hemisphere sudden stratosphere warming event, we additionally investigate how interannual variability in the timing of the SW2 minimum is related to the timing of the seasonal transition in the middle atmosphere. Our investigation of the SW2 minimum is performed using long-term SD-WACCMX simulations along with specular meteor radar observations. The results provide insight into the role of the seasonal transition of the zonal mean zonal winds on generating the SW2 minimum at middle to high latitudes in the Northern Hemisphere. Furthermore, they reveal how the timing of the seasonal transition of middle atmosphere zonal mean zonal winds modulates the timing of the SW2 in the MLT at middle to high latitudes in the Northern Hemisphere.
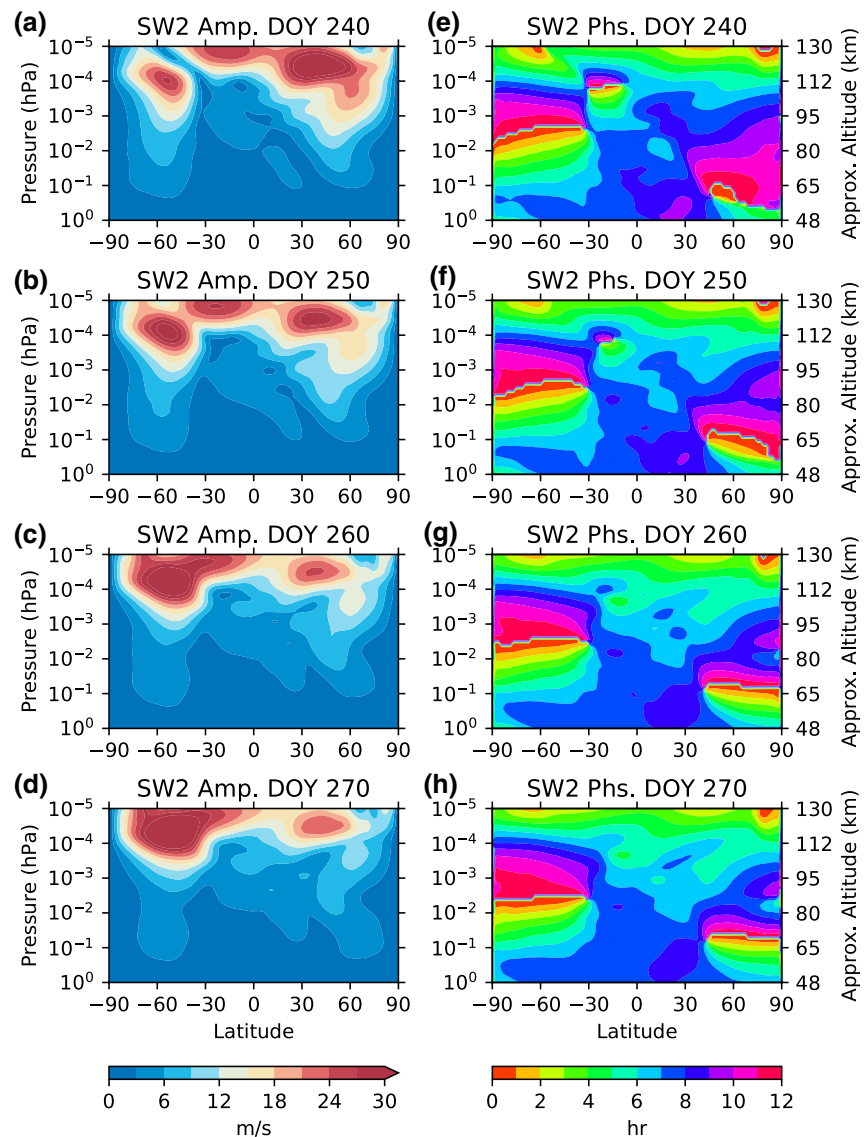
Figure 2. SD-WACCMX climatological SW2 amplitude in zonal wind on day of year (a) 240, (b) 250, (c) 260, and (d) 270. (e)–(h) Same as (a)–(d) except for the SW2 phase. Results are based on the 1980–2016 average. SD-WACCMX, Specified Dynamics Whole Atmosphere Community Climate Model with thermosphere-ionosphere eXtension.

2. WACCMX Simulations

WACCMX is a whole atmosphere chemistry climate model that incorporates ionosphere and thermosphere processes (H.-L. Liu et al., 2018). WACCMX extends from the surface to the upper thermosphere (4.1×10^{-10} hPa, 500–700 km depending on solar activity). Below the lower thermosphere, the model is based on the Whole Atmosphere Community Climate Model (WACCM) version 4 (Marsh et al., 2013), which itself is based on the Community Atmosphere Model (CAM) version 4 (Neale et al., 2013). A detailed description of the additional ionosphere and thermosphere processes that are included in WACCMX can be found in H.-L. Liu et al. (2018). An initial validation of WACCMX, including the migrating and nonmigrating tides, was performed by J. Liu et al. (2018).

The present study analyzes specified dynamics WACCMX (SD-WACCMX) simulations that cover the time period 1980–2016, as well as the year 2019. In SD-WACCMX, the model meteorology is constrained to the NASA MERRA-2 reanalysis up to ~50 km using the technique described in Smith et al. (2017). Above ~50 km the model is free-running, and is not constrained by the reanalysis. By constraining the mod-
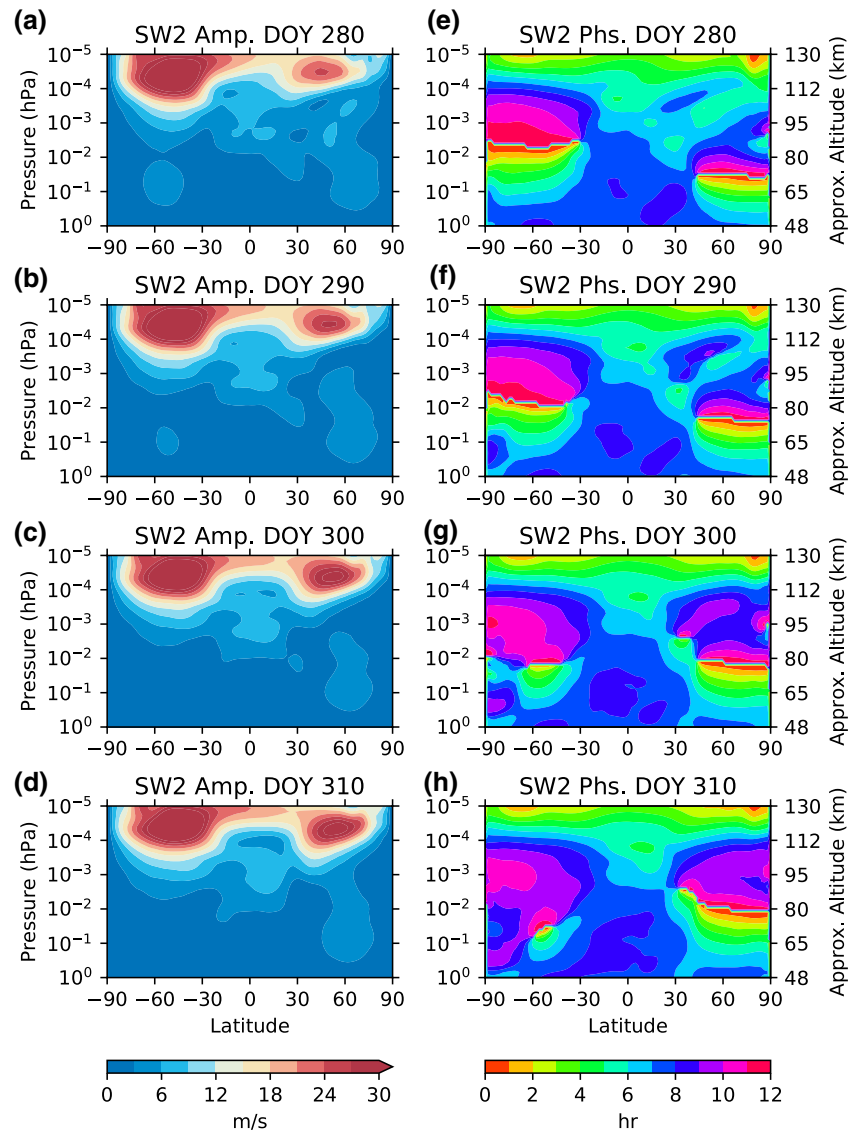
Figure 3. SD-WACCMX climatological SW2 amplitude in zonal wind on day of year (a) 280, (b) 290, (c) 300, and (d) 310. (e)–(h) Same as (a)–(d) except for the SW2 phase. Results are based on the 1980–2016 average. SD-WACCMX, Specified Dynamics Whole Atmosphere Community Climate Model with thermosphere-ionosphere eXtension.

el meteorology to the MERRA-2 reanalysis, the SD-WACCMX simulations reproduce the historical variability of the atmosphere during the analyzed time period. The analysis primarily focuses on output from SD-WACCMX simulations that cover the time period from 1980-2016 (https://doi.org/10.26024/5b58-nc53). We have, however, extended the analysis to include a SD-WACCMX simulation for 2019 due to the minor SSW, and early winter to summer transition, that occurred in the Southern Hemisphere during 2019. For the present study, we use SD-WACCMX output at a three hourly cadence, and perform a least squares fitting to obtain the daily SW2 amplitude and phase. A 10-day running mean is subsequently applied.

3. Radar Observations

Measurements obtained from five specular meteor radars (SMRs) are considered in this study. To improve the data coverage in time, the meteor detections from Andenes (69°N, 16°E) and Tromsø (69°N, 18°E) SMRs were combined following the procedure described in Chau et al. (2017). The same procedure was used to combine measurements provided by the SMRs located at Juliusruh (54°N, 13°E) and Collm (51°N, 13°E)

(e.g., Hoffmann et al., 2010; Jacobi, 2012). For the period 1999–2002, data from the Esrange (67°N, 20°E) monostatic system was used (e.g., Sandford et al., 2006). Hourly horizontal winds were estimated every 2 km in altitude over the three observed volumes, by means of an all-sky fit method (Hocking et al., 2001; Holdsworth et al., 2004).

The estimated hourly zonal (u) and meridional (v) winds were further processed in order to obtain information about tides and other large scale waves. Assuming that they result from a linear superposition of a mean background flow and different period waves, the following expression can be independently fit to u and v (e.g., Conte et al., 2019; Sandford et al., 2006),

$$(u + \sigma_u, v + \sigma_v) = (u_0, v_0) + \sum_{i=1}^{5}(a_{u_i}, a_{v_i})\cos\left(2\pi \frac{t}{T_i}\right) + (b_{u_i}, b_{v_i})\sin\left(2\pi \frac{t}{T_i}\right) \qquad (1)$$

Here, u_0 and v_0 are the mean zonal and meridional winds, respectively; σ_u and σ_v are the statistical uncertainties of the zonal and meridional wind estimates, respectively; T_i is the period for each considered wave (i.e., $T_1 = 48$ h, $T_2 = 24$ h, $T_3 = 12$ h, $T_4 = 8$ h, and $T_5 = 12.42$ h, for the quasi 2-day wave, the solar diurnal, semidiurnal and terdiurnal tides, and the lunar semidiurnal tide, respectively); $a_{\alpha_i}, b_{\alpha_i}$ are coefficients of the waves amplitudes for each wind component ($\alpha = u, v$); and t is the time in hours. Equation 1 was solved using a least squares method with a running window of 21 days shifted by 1 day. The length of 21 days was selected in order to separate the semidiurnal solar (12 h) and lunar (12.42 h) tides. Note that because the radar observations are for a single location, the semidiurnal solar tide observed by the radars (denoted S2) is the total semidiurnal tide, and includes contributions from migrating and nonmigrating tides. However, He and Chau (2019) found that the S2 at middle to high latitudes in the Northern Hemisphere will be primarily dominated by the SW2, with smaller contributions from nonmigrating tides.

4. Results and Discussion

4.1. Climatology

The amplitude and phase of the climatological SW2 in zonal wind every 10 days from day of year 240–310 are shown in Figures 2 and 3. Corresponding vertical profiles of the unwrapped tidal phase at 60°N are shown in Figure 4. At middle latitudes (30–60°N) in the Northern Hemisphere MLT there is a weakening of the SW2 between days 240–270, followed by an enhancement over the next ~30 days. This is consistent with the results shown in Figure 1. The results in Figures 2–4 reveal that the amplitude changes at middle to high latitudes in the Northern Hemisphere are accompanied by notable changes in the tidal phase, especially between 1 and 10^{-3} hPa. The phase changes indicate a reduction in the tidal vertical wavelength, which coincides with the amplitude reduction. Between days 240 and 270 the SW2 vertical wavelength in the mesosphere near 60°N decreases from ~100 to ~40 km. An increase in vertical wavelength also accompanies the increasing amplitude after day ~280. The decrease in vertical wavelength may be due to the increased excitation of higher order tidal modes, which have a shorter vertical wavelength, by ozone heating near equinox (Forbes & Garrett, 1978; Groves, 1982). Since shorter vertical wavelength tides are more effectively damped due to eddy and molecular diffusion (e.g., Forbes & Garrett, 1979), the decrease in SW2 amplitude in the Northern Hemisphere may thus partly be due to the decreased vertical wavelength.

In order to further understand the source of the SW2 minimum at middle to high latitudes in the Northern Hemisphere around September equinox, Figure 5 presents the climatological zonal mean zonal wind every 10 days from day of year 240–310. The zonal mean zonal winds display
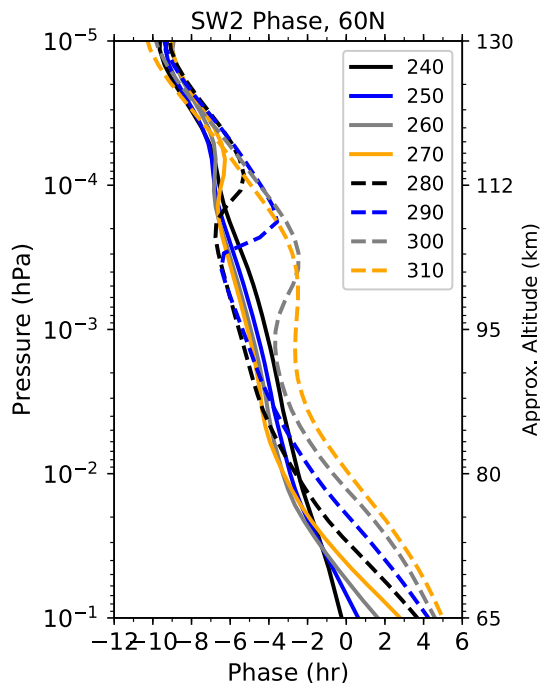

Figure 4. SD-WACCMX SW2 phase in zonal wind at 60°N on day of year 240, 250, 260, 270, 280, 290, 300, and 310. Results are based on the 1980–2016 average. SD-WACCMX, Specified Dynamics Whole Atmosphere Community Climate Model with thermosphere-ionosphere eXtension.
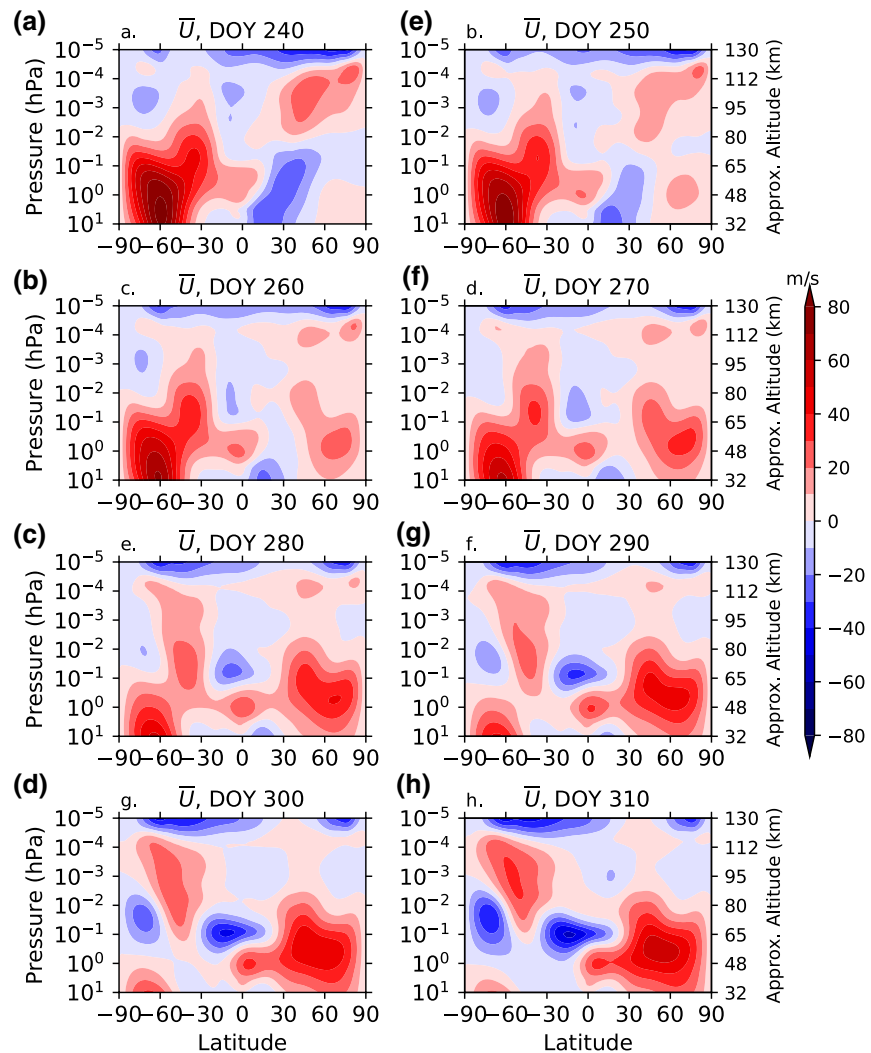
Figure 5. SD-WACCMX climatological zonal mean zonal wind on day of year (a) 240, (b) 250, (c) 260, (d) 270, (e) 280, (f) 290, (g) 300, and (h) 310. Results are based on the 1980–2016 average. SD-WACCMX, Specified Dynamics Whole Atmosphere Community Climate Model with thermosphere-ionosphere eXtension.

the expected seasonal climatology as the stratosphere and mesosphere transition from winter to summer in the Southern Hemisphere and summer to winter in the Northern Hemisphere. In particular, the strong stratospheric eastward winds in the Southern Hemisphere gradually weaken and then transition to westward. This is accompanied by a shift in the high latitude Southern Hemisphere MLT winds from westward to eastward. The opposite behavior occurs in the Northern Hemisphere, with winds in the stratosphere becoming increasingly eastward, and high latitude MLT winds transitioning from eastward to westward. As the seasonal transition occurs, there is a period around days 270–290 when the zonal mean zonal winds are weak and considerably more hemispherically symmetric compared to before or after this time period. This brief period of weak and hemispherically symmetric zonal mean zonal winds will significantly alter tidal propagation conditions, and is important to bear in mind during the subsequent discussions.

It is useful to decompose the SW2 into Hough modes (Chapman & Lindzen, 1970), which can provide insight into how different tidal modes vary during the September equinox transition. The amplitude of the first two symmetric ((2,2) and (2,4)) and antisymmetric ((2,3) and (2,5)) Hough modes, along with their vector sum, at 10^{-3} hPa are shown in Figure 6. The results in Figure 6 are obtained based on fitting the SW2 in zonal wind to the first 10 symmetric and antisymmetric Hough modes; however, we only show the first two symmetric and antisymmetric Hough modes as reconstruction of the SW2 from these
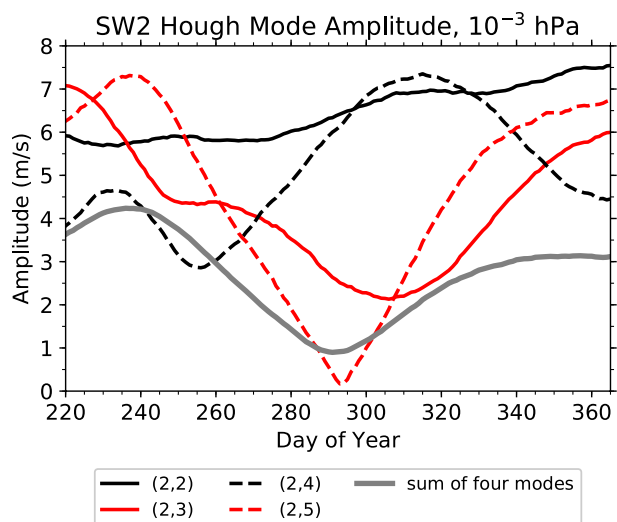
Figure 6. Amplitude of the first four Hough modes of SW2 at 10^{-3} hPa (~95 km), and their vector sum, based on the SD-WACCMX 1980–2016 average. SD-WACCMX, Specified Dynamics Whole Atmosphere Community Climate Model with thermosphere-ionosphere eXtension.

modes is sufficient to capture the salient features of the SW2 variability shown in Figures 1–3 (not shown). The results in Figure 6 reveal that there are notable changes in the (2,3), (2,4), and (2,5) modes around September equinox. In particular, the antisymmetric modes gradually decrease, obtaining minima around day 300 before gradually increasing. The second symmetric mode, (2,4), exhibits the opposite behavior and has a maximum around day 315. The first symmetric mode, (2,2), displays little variability, which is consistent with previous results (e.g., Forbes & Vial, 1989). The sum of the first two symmetric and antisymmetric modes has a minimum around day 290. As will be discussed in more detail later, the timing of this minimum results from a combination of amplitude and phase changes of the different modes. The results in Figures 2–6 combined can provide insight into the source of the SW2 minimum that occurs at middle to high latitudes in the Northern Hemisphere around September equinox. Concerning first the decreased amplitude of the antisymmetric modes, we consider this to be the result of the seasonal changes in the zonal mean zonal winds. The antisymmetric modes of SW2 are primarily generated by mode coupling that occurs due to the presence of meridional gradients in temperature and zonal winds (Forbes & Garrett, 1979; Lindzen & Hong, 1974). As shown in Figure 5, the meridional gradients are small (i.e., the zonal mean zonal winds are largely hemispherically symmetric) around the September equinox. This will lead to a reduction in the (2,3) and (2,5) modes. At

the same time as the antisymmetric modes are decreasing, the second symmetric mode increases. As discussed previously, this is likely due to the increased ozone forcing of the (2,4) mode around equinox, and may also be due to favorable propagation conditions in the near zero zonal mean zonal winds that occur around equinox. Though the (2,4) mode increases, it is insufficient to compensate for the decreased antisymmetric amplitudes. Last, we note that the decreased SW2 amplitude is confined to the Northern Hemisphere (e.g., Figure 1a). This is the result of constructive/destructive interference between the different symmetric and antisymmetric modes, which leads to reduced amplitudes in the Northern Hemisphere, but not in the Southern Hemisphere. The constructive/destructive interference is illustrated in
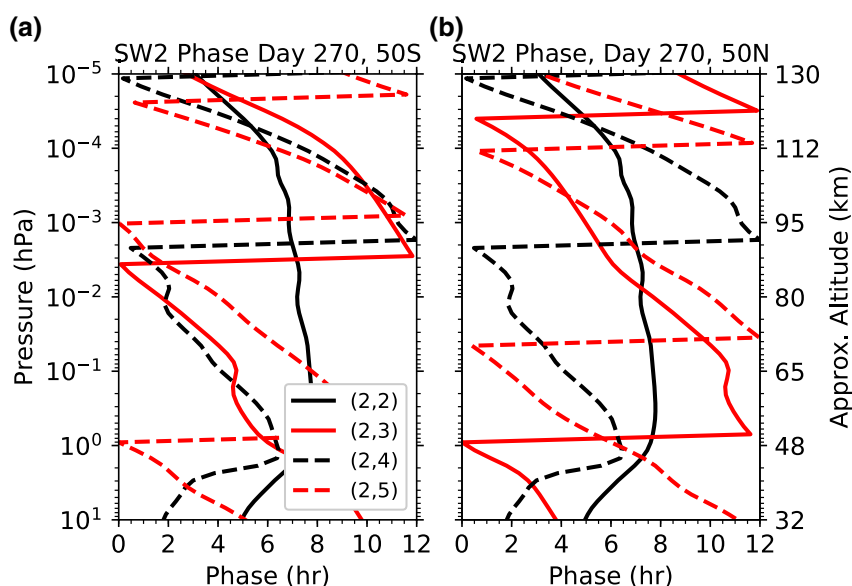

Figure 7. Phase of the first four Hough modes on day of year 270 at (a) 50°S and (b) 50°N. The results are based on the SD-WACCMX 1980–2016 average. SD-WACCMX, Specified Dynamics Whole Atmosphere Community Climate Model with thermosphere-ionosphere eXtension.
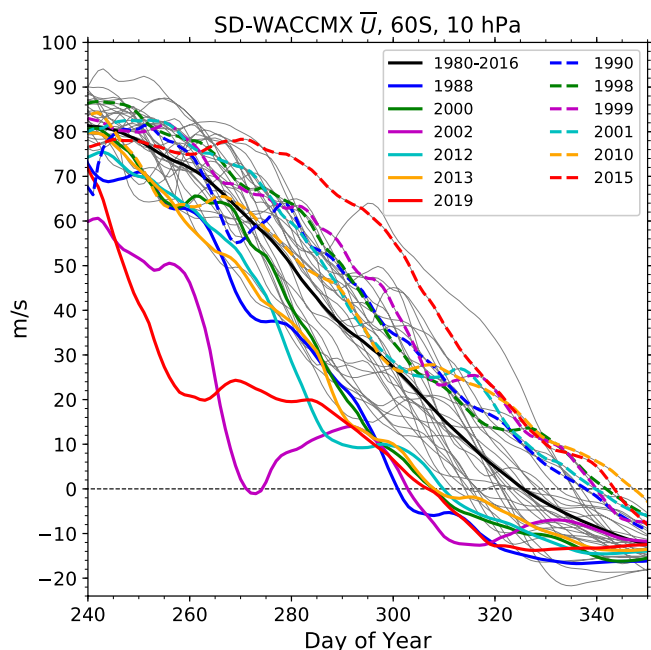
Figure 8. SD-WACCMX zonal mean zonal wind at 60°S and 10 hPa. Thin gray lines are the zonal mean zonal wind for individual years, and the solid black line indicates the 1980–2016 climatological average. Years with the six earliest and latest transitions from eastward to westward zonal mean zonal winds are indicated by the colored solid and dashed lines, respectively. SD-WACCMX, Specified Dynamics Whole Atmosphere Community Climate Model with thermosphere-ionosphere eXtension.

Figure 7, which shows the phases of the different Hough modes at 50°S (Figure 7a) and 50°N (Figure 7b) on day 270. The in-phase relationship of the Hough modes in the Southern Hemisphere MLT means that the enhancement in the (2,4) mode compensates for the decrease in the antisymmetric modes. However, in the Northern Hemisphere MLT, these Hough modes are out of phase, leading to destructive interference among the different modes and an overall reduction in the tidal amplitudes.

4.2. Interannual Variability

We now turn our attention to how interannual variations in the timing of the seasonal transition of the zonal mean zonal winds influences the SW2 minimum at middle to high latitudes in the Northern Hemisphere. As an indicator of the timing of the seasonal transition, we use the zonal mean zonal winds at 60°S and 10 hPa. The SD-WACCMX simulated winds at 60°S and 10 hPa during the years 1980–2016 and 2019 are shown in Figure 8. The solid black line indicates the climatological mean, and the colored solid and dashed lines indicate the six earliest and latest seasonal transitions from eastward to westward zonal mean zonal winds, respectively. The climatological transition date is around day 325. In contrast, the zonal mean zonal winds reverse between days 300–310 in the six early transition years, and days 340–350 during the late transition years. As discussed later, the timing of the wind reversal in the Southern Hemisphere stratosphere is indicative of the timing of the seasonal transition of the winds throughout the middle atmosphere. There is thus considerable interannual variability in the timing of the seasonal transition throughout the middle atmosphere. Throughout the following, the six earliest and latest seasonal transition years will be used to understand how the timing of

the seasonal transition in the middle atmosphere winds influences the SW2 minimum in the Northern Hemisphere. Note that in the present study we are interested in the response of the SW2 to the early or late seasonal transition, and thus do not investigate the source mechanisms that drive the interannual variability in the seasonal transition. We do, however, note that the transition date is influenced by wave forcing with years of stronger wave forcing, and often major or minor sudden stratospheric warming events, having an earlier seasonal transition.

The timing of the seasonal transition in the Southern Hemisphere stratosphere shown in Figure 8 is indicative of the seasonal transition throughout the middle atmosphere. Figure 9 shows the zonal mean zonal winds averaged between 40 and 60°N and 40–60°S for the early (Figure 9a and 9c) and late (Figure 9b and 9d) transition years. As expected, the zonal mean zonal winds in the Southern Hemisphere stratosphere transition from eastward to westward ~20 days earlier in the early transition years compared to the late transition years. The earlier transition to westward winds in the stratosphere is accompanied by an earlier strengthening of the eastward winds in the MLT, which is due to the role of the stratospheric winds on filtering the gravity waves that influence the MLT circulation. In the Northern Hemisphere (Figure 9a and 9b), the zonal mean zonal winds in the stratosphere are generally similar in the early and late transition years, especially with regards to the timing of the wind reversal. There is, however, an earlier formation of the westward winds in the MLT in the early transition years compared to the late transition years. The earlier transition in the Northern Hemisphere MLT is considered to be due to the interhemispheric coupling that is known to occur between the high latitude wintertime stratosphere and summer mesosphere (Körnich & Becker, 2010; Smith et al., 2020).

As discussed previously, the SW2 minimum in the Northern Hemisphere is largely controlled by the occurrence of hemispherically symmetric zonal mean zonal winds around September equinox. The results shown in Figure 9 indicate that the timing of when the winds are most hemispherically symmetric will be
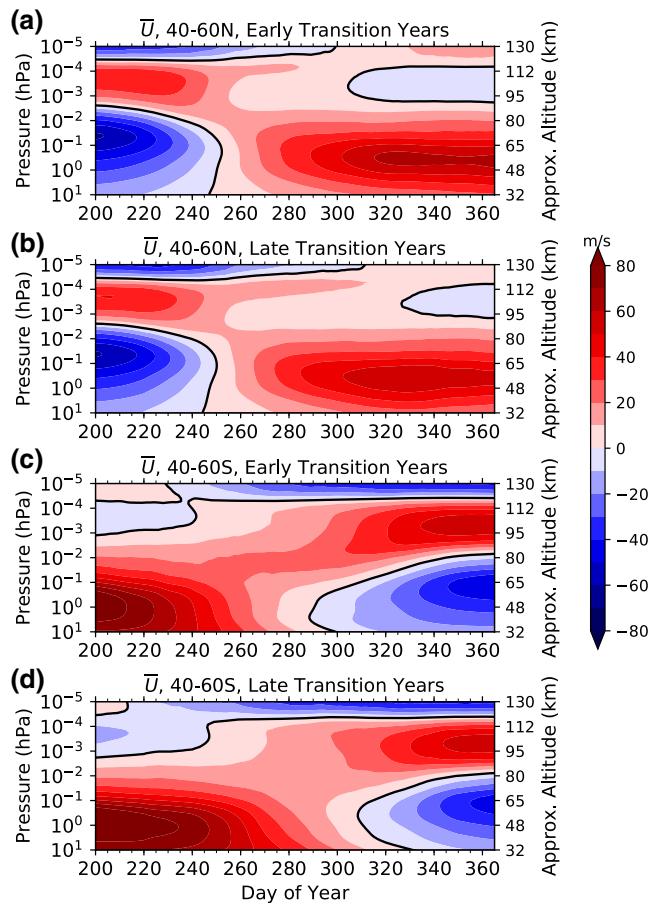
Figure 9. Zonal mean zonal winds averaged between 40 and 60°N for the (a) early, and (b) late transition years. (c)–(d) Same as (a)–(b) except averaged between 40 and 60°S. SD-WACCMX, Specified Dynamics Whole Atmosphere Community Climate Model with thermosphere-ionosphere eXtension.

different during the early and late transition years. This is more clearly demonstrated in Figure 10, which shows the quantity $\frac{1}{2}|U_n - U_s|$ averaged between 10 and 10^{-3} hPa, where U_n and U_s are the mean zonal mean zonal winds between 40–60°N and 40–60°S, respectively. This quantity will be minimum when the winds are most symmetric (i.e., $U_n \approx U_s$). Figure 10 shows the climatological value (black line), standard deviation (gray shading), as well as the early (Figure 10a) and late (Figure 10b) transition years. It is evident in Figure 10 that climatologically the middle atmosphere winds are most symmetric around days 270–280, which is generally consistent with the climatological timing of the SW2 minimum in the Northern Hemisphere MLT. Furthermore, the results in Figure 10 demonstrate that the zonal mean zonal winds in the middle atmosphere are more symmetric earlier compared to climatology (and less symmetric later) during the early transition years, with the opposite occurring in the late transition years. This indicates that, though defined based on the timing of the transition of the zonal mean zonal winds in the Southern Hemisphere stratosphere, the early and late transition years exhibit different timing of the seasonal transition, and hemispheric symmetry, of the winds throughout the middle atmosphere.

An example of the impact of the timing of the seasonal transition on the SW2 minimum in the middle to high latitude Northern Hemisphere is shown in Figure 11. Figure 11 shows the SW2 averaged between 40 and 60°N during 2002 (11a, early transition year), 2015 (11b, late transition year), and the 1980–2016 climatology (11c). The results in Figure 11 clearly illustrate that the SW2 minimum occurs earlier than the climatological minimum in 2002, and later than the climatological minimum in 2015. There thus appears to be a relationship between the timing of the seasonal transition and the timing of the SW2 minimum, with an earlier seasonal transition corresponding to an earlier SW2 minimum. This is further supported by the results in Figure 12, which shows the timing of the SW2 minimum at different pressure levels for the SD-WACCMX climatology (black line), early transition years ("x" symbols) and late transition years ("o" symbols). Note that the gray shading indicates one standard deviation of the SW2 minimum date for the period 1980–2016, including the six early and late transition years. Focusing first on the early transition years, it is clear that the SW2 minimum occurs ~10–15 days earlier than climatology, with the date of the minima occurring outside of one standard deviation for nearly all years and pressure levels. Results for the late transition years are perhaps less clear, though it is evident that the SW2 minima tend to occur slightly later (~5–10 days on average) than the climatological minimum. Based on these results, we conclude that an earlier seasonal transition in the middle atmosphere winds leads to earlier occurrence of the SW2 minimum at middle to high latitudes in the Northern Hemisphere. Likewise a later seasonal transition will tend to lead to a later occurrence of the SW2 minimum. The response does, however, appear to be stronger for the early transition years compared to the late transition years.

We complement the SD-WACCMX simulation results with SMR observations at middle to high latitudes in the Northern Hemisphere during the early and late transition years. Figure 13 shows the average total semidiurnal tide (S2) during early (left panels) and late (right panels) transition years. Though the S2 contains contributions from both the SW2 and nonmigrating tides, it is dominated by the SW2 at middle to high latitudes in the Northern Hemisphere (He & Chau, 2019). Note that due to limited observations, the early transition years are averaged for 2000, 2002, 2012, 2013, and 2019 for the Northern Scandanavia radars (Andenes, Esrange, and Tromsø) and 2012, 2013, and 2019 for the radars in Northern Germany (Collm and Juliusruh). Late transition years are similarly limited to only 1999, 2001, 2010
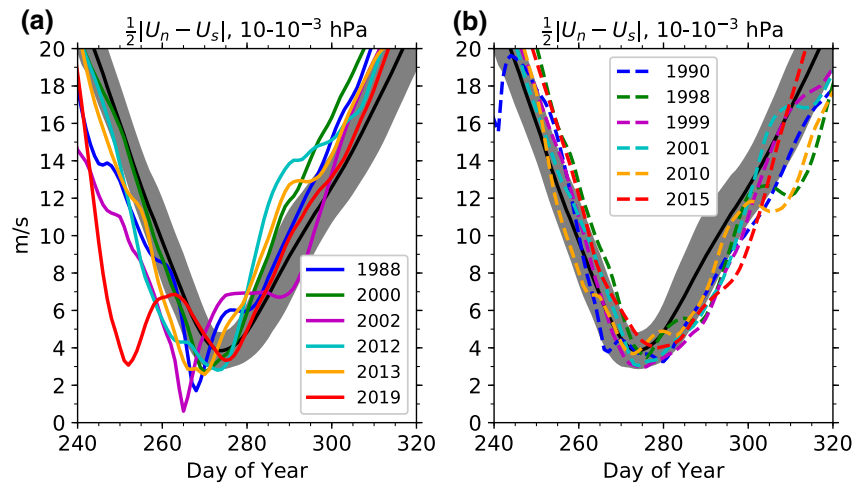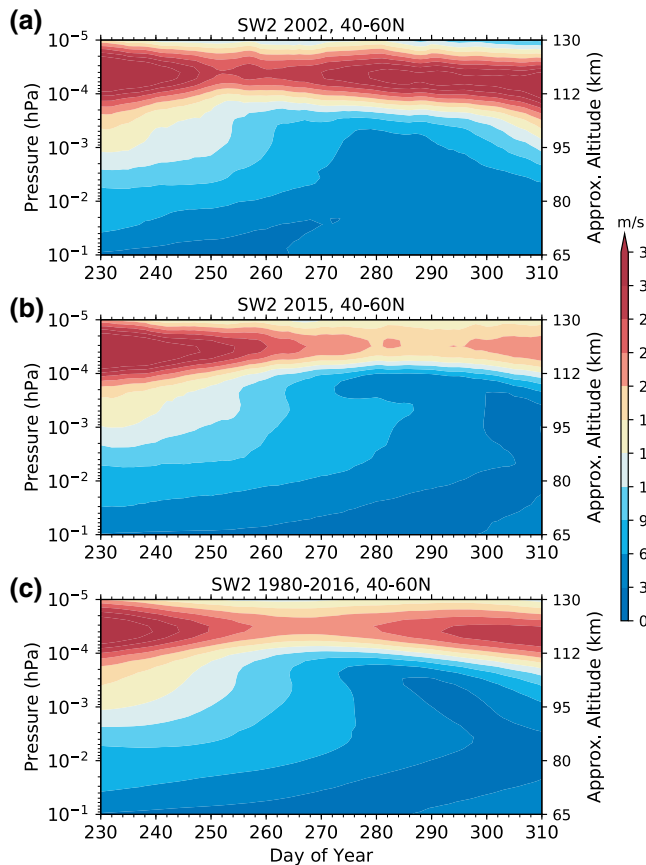
Figure 10. SD-WACCMX zonal mean zonal wind hemisphere symmetry averaged between 10 and 10^{-3} hPa for (a) early, and (b) late transition years. The 1980–2016 climatological average and one standard deviation are indicated by the black line and gray shading, respectively. The hemisphere symmetry is defined as $\frac{1}{2}|U_n - U_s|$, where U_n and U_s are the zonal mean zonal wind averaged between 40–60°N and 40–60°S, respectively. SD-WACCMX, Specified Dynamics Whole Atmosphere Community Climate Model with thermosphere-ionosphere eXtension.

Figure 11. SD-WACCMX SW2 amplitude in zonal wind averaged between 40 and 60°N for (a) 2002, (b) 2015, and (c) the 1980–2016 average. SD-WACCMX, Specified Dynamics Whole Atmosphere Community Climate Model with thermosphere-ionosphere eXtension.

and 2015 for Northern Scandinavia, and 2010 and 2015 for Northern Germany. Similar to what has been shown in previous studies (Chau et al., 2015; Conte et al., 2018), the radar observations exhibit a pronounced minimum in the S2 amplitude around September equinox. Comparison of the S2 during early and late transition years reveals that, consistent with the SD-WACCMX simulations, the S2 minimum occurs earlier in the early transition years and later in the late transition years. In particular, it is clear that the S2 amplitude quickly decreases around day 250–260 in the early transition years compared to around day 280 in the late transition years. The increase in the S2 amplitude that occurs 20–30 days later also occurs earlier in the early transition years compared to the late transition years. A latitudinal dependence to the S2 minimum is also evident in Figure 13, with S2 minimum being shorter at 50–55°N (Northern Germany) compared to ~70°N (Northern Scandinavia). This latitudinal dependence is also consistent with the latitudinal dependence of the SW2 minimum in the SD-WACCMX simulations (Figure 1).The radar results thus confirm the results of the SD-WACCMX simulations.

As discussed in Section 4.1, the seasonal transition of the zonal mean zonal winds impacts the different modes of SW2. Figures 14 and 15 show the amplitudes of the first two symmetric and antisymmetric Hough modes at 10^{-3} hPa for the early and late transition years, respectively. The results in Figure 14 illustrate that the (2,3), (2,4), and (2,5) modes display a clear response to the earlier seasonal transition in the Southern Hemisphere stratosphere. In particular, the first and second antisymmetric modes minima and the second symmetric mode maximum occur earlier compared to climatology. The earlier occurrence of the (2,3) and (2,5) minima and (2,4) maximum can largely be attributed to the earlier occurrence of symmetric zonal mean zonal winds during the early transition years (Figure 10). The late transition years (Figure 15) tend to show the opposite response, though it is less pronounced compared to the early transition years. In the late transition
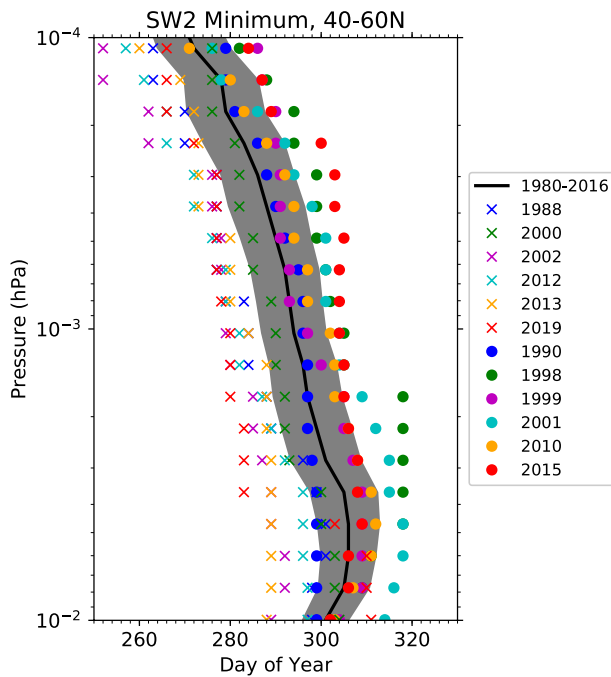
Figure 12. Day of year when the minimum SW2 amplitude (averaged between 40 and 60°N) occurs. Solid black line indicates the 1980–2016 average, and the gray shading indicates one standard deviation. Colored "x" and "o" symbols indicate individual early and late transition years, respectively.

years, the response is most apparent in the antisymmetric modes, especially the (2,5) mode, which shows a slightly later minima compared to climatology. Unlike the early transition years, the second symmetric mode does not display a clear difference compared to climatology in the late transition years. This may partly explain the less definitive results for the timing of the SW2 minima in the late transition years compared to climatology in Figure 12.

Based on these results, we can summarize the impact of the seasonal transition in the middle atmosphere zonal mean zonal winds on the timing of the SW2 minimum at middle to high latitudes in the Northern Hemisphere as follows. The timing of the seasonal transition in the Southern Hemisphere stratosphere, which we use to define the early and late transition years, is related to the seasonal transition throughout the middle atmosphere. This includes the timing of when the middle atmosphere zonal mean zonal winds are most hemispherically symmetric. As discussed with regards to the SW2 climatology (Section 4.1), the seasonal transition of the winds throughout the middle atmosphere influences the generation and propagation of different Hough modes, which constructively/destructively combine to generate the SW2 minimum. An earlier or later seasonal transition of the zonal mean zonal winds, and the corresponding earlier or later occurrence of hemispherically symmetric winds, will thus lead to a shift in the timing of the Hough modes (Figures 14 and 15), ultimately generating a shift in the timing of the SW2 minimum.
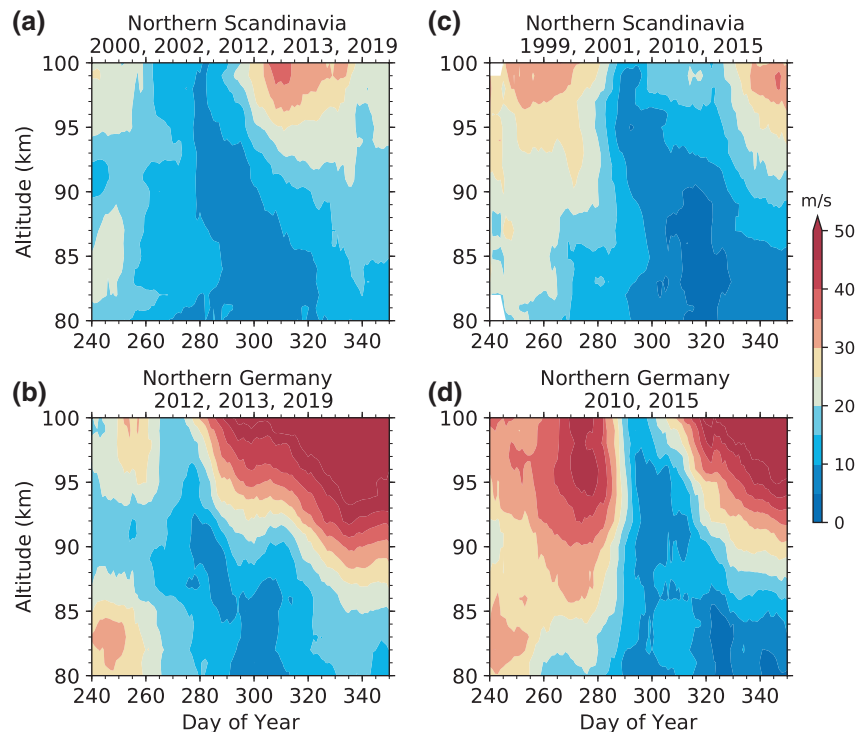

Figure 13. Amplitude of the total semidiurnal tide (S2) in specular meteor radar observations for (a) Northern Scandinavia (Andenes, Tromsø, and Esrange), and (b) Northern Germany (Collm and Juliusruh) during early transition years. (c)–(d) Same as (a)–(b) except for late transition years.
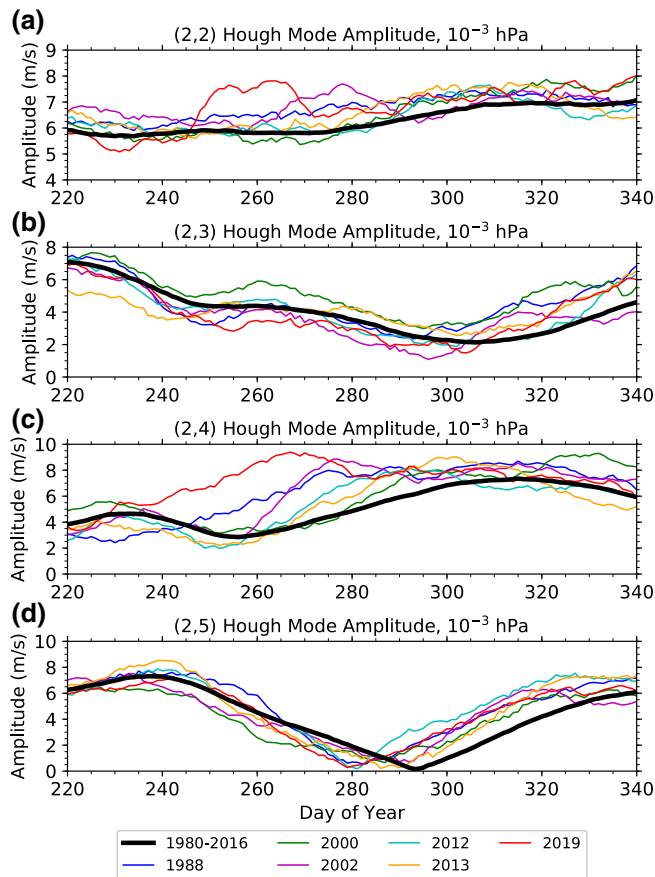
Figure 14. Amplitude of the SW2 (a) (2,2), (b) (2,3), (c) (2,4), and (d) (2,5) Hough modes at 10^{-3} hPa ($\sim$95 km) for the climatological average (black line) and early transition years (colored lines).
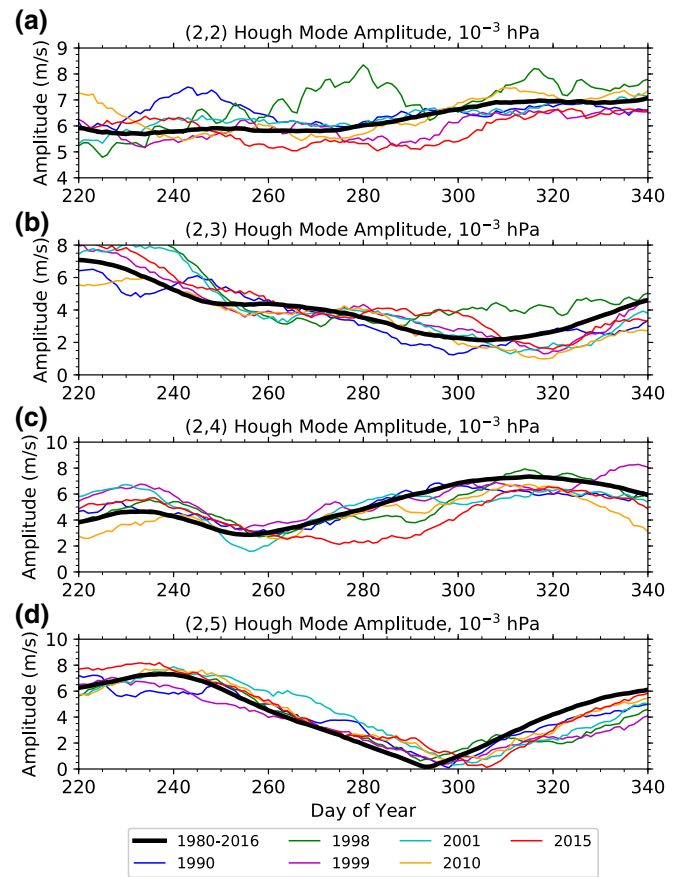
Figure 15. Amplitude of the SW2 (a) (2,2), (b) (2,3), (c) (2,4), and (d) (2,5) Hough modes at 10^{-3} hPa ($\sim$95 km) for the climatological average (black line) and late transition years (colored lines).

5. Conclusions

The present study investigates the formation of the deep SW2 minimum that lasts for 20–30 days at middle to high latitudes in the Northern Hemisphere around September equinox. Analysis of SD-WACCMX simulations reveals that the SW2 minimum is primarily related to the seasonal transition of the zonal mean zonal winds in the middle atmosphere, which alters the generation and propagation of different SW2 tidal modes. In particular, there is a notable reduction in the amplitude of antisymmetric modes due to the zonal mean zonal winds being more hemispherically symmetric around equinox. The constructive/destructive interaction among the different modes leads to the SW2 minimum at middle to high latitudes in the Northern Hemisphere. Furthermore, the timing of the SW2 minimum has considerable interannual variability, with yearly minima occurring $\sim$10–20 days before or after the climatological minimum. The results demonstrate that the shift in timing of the SW2 minimum is related to the timing of the seasonal transition of the zonal mean zonal winds in the middle atmosphere.

It is important to note that the SW2 at MLT altitudes can play an important role in coupling the lower/middle and upper atmospheres. Specifically, the SW2 can influence the electrodynamics of the low-latitude ionosphere (Millward et al., 2001), and its dissipation can alter the dynamics and composition of the lower thermosphere (Pedatella et al., 2016). It remains to be investigated how the SW2 minimum may impact the upper atmosphere. The interannual variations in the timing of the SW2 minimum could also serve as a mechanism for generating interannual variations in the ionosphere and thermosphere. This may impact, for example, the variability of the ionosphere during and after the recent 2019 Southern Hemisphere sudden stratosphere warming event, which exhibited an early seasonal transition.

References

Akmaev, R. A., & Shved, G. M. (1980). Modelling of the composition of the lower thermosphere taking account of the dynamics with applications to tidal variations of the [OI] 5577 Å airglow. *Journal of Atmospheric and Terrestrial Physics*, *42*(8), 705–716. https://doi.org/10.1016/0021-9169(80)90054-9

Andrews, D. G., Holton, J. R., & Leovy, C. B. (1987). *Middle atmosphere dynamics*. Academic Press.

Angelats i Coll, M., & Forbes, J. M. (2002). Nonlinear interactions in the upper atmosphere: The s = 1 and s = 3 nonmigrating semidiurnal tides. *Journal of Geophysical Research*, *107*(A8), SIA 3–1–SIA 3–15. https://doi.org/10.1029/2001JA900179

Chapman, S., & Lindzen, R. (1970). *Atmospheric tides*. Dordrecht, Holland: Reidel.

Chau, J. L., Hoffmann, P., Pedatella, N. M., Matthias, V., & Stober, G. (2015). Upper mesospheric lunar tides over middle and high latitudes during sudden stratospheric warming events. *Journal of Geophysical Research: Space Physics*, *120*, 3084–3096. https://doi.org/10.1002/2015JA020998

Chau, J. L., Stober, G., Hall, C. M., Tsutsumi, M., Laskar, F. I., & Hoffmann, P. (2017). Polar mesospheric horizontal divergence and relative vorticity measurements using multiple specular meteor radars. *Radio Science*, *52*(7), 811–828. https://doi.org/10.1002/2016RS006225

Conte, J. F., Chau, J. L., Laskar, F. I., Stober, G., Schmidt, H., & Brown, P. (2018). Semidiurnal solar tide differences between fall and spring transition times in the Northern Hemisphere. *Annales Geophysicae*, *36*(4), 999–1008. https://doi.org/10.5194/angeo-36-999-2018

Conte, J. F., Chau, J. L., & Peters, D. H. W. (2019). Middle- and high-latitude mesosphere and lower thermosphere mean winds and tides in response to strong polar-night jet oscillations. *Journal of Geophysical Research: Atmospheres*, *124*, 9262–9276. https://doi.org/10.1029/2019JD030828

Eckermann, S. D., & Marks, C. J. (1996). An idealized ray model of gravity wave-tidal interactions. *Journal of Geophysical Research*, *101*(D16), 21195–21212. https://doi.org/10.1029/96JD01660

Fesen, C. G., Crowley, G., Roble, R. G., Richmond, A. D., & Fejer, B. G. (2000). Simulation of the pre-reversal enhancement in the low latitude vertical ion drifts. *Geophysical Research Letters*, *27*(13), 1851–1854. https://doi.org/10.1029/2000GL000061

Forbes, J. M., & Garrett, H. B. (1978). Thermal excitation of atmospheric tides due to insolation absorption by O3 and H2O. *Geophysical Research Letters*, *5*(12), 1013–1016. https://doi.org/10.1029/GL005i012p01013

Forbes, J. M., & Garrett, H. B. (1979). Theoretical studies of atmospheric tides. *Reviews of Geophysics*, *17*(8), 1951–1981. https://doi.org/10.1029/RG017i008p01951

Forbes, J. M., Roble, R. G., & Fesen, C. G. (1993). Acceleration, heating, and compositional mixing of the thermosphere due to upward propagating tides. *Journal of Geophysical Research*, *98*(A1), 311–321. https://doi.org/10.1029/92JA00442

Forbes, J. M., & Vial, F. (1989). Monthly simulations of the solar semidiurnal tide in the mesosphere and lower thermosphere. *Journal of Atmospheric and Terrestrial Physics*, *51*(7), 649–661. https://doi.org/10.1016/0021-9169(89)90063-9

Fritts, D. C., & Vincent, R. A. (1987). Mesospheric momentum flux studies at Adelaide, Australia: Observations and a gravity wave–tidal interaction model. *Journal of the Atmospheric Sciences*, *44*(3), 605–619. 10.1175/1520-0469(1987)044⟨0605:MMFSAA⟩2.0.CO;2

Groves, G. V. (1982). Hough components of ozone heating. *Journal of Atmospheric and Terrestrial Physics*, *44*(2), 111–121. https://doi.org/10.1016/0021-9169(82)90114-3

Hagan, M. E., Vial, F., & Forbes, J. M. (1992). Variability in the upward propagating semidiurnal tide due to effects of QBO in the lower atmosphere. *Journal of Atmospheric and Terrestrial Physics*, *54*(11), 1465–1474. https://doi.org/10.1016/0021-9169(92)90153-C

He, M., & Chau, J. L. (2019). Mesospheric semidiurnal tides and near-12,h waves through jointly analyzing observations of five specular meteor radars from three longitudinal sectors at boreal midlatitudes. *Atmospheric Chemistry and Physics*, *19*(9), 5993–6006. https://doi.org/10.5194/acp-19-5993-2019

He, M., Chau, J. L., Stober, G., Hall, C. M., Tsutsumi, M., & Hoffmann, P. (2017). Application of Manley-Rowe relation in analyzing nonlinear interactions between planetary waves and the solar semidiurnal tide during 2009 sudden stratospheric warming event. *Journal of Geophysical Research: Space Physics*, *122*, 10710–783795 https://doi.org/10.1002/2017JA024630

Hocking, W. K., Fuller, B., & Vandepeer, B. (2001). Real-time determination of meteor-related parameters utilizing modern digital technology. *Journal of Atmospheric and Solar-Terrestrial Physics*, *63*(2), 155–169. https://doi.org/10.1016/S1364-6826(00)00138-3

Hoffmann, P., Becker, E., Singer, W., & Placke, M. (2010). Seasonal variation of mesospheric waves at northern middle and high latitudes. *Journal of Atmospheric and Solar-Terrestrial Physics*, *72*(14), 1068–1079. https://doi.org/10.1016/j.jastp.2010.07.002

Holdsworth, D. A., Reid, I. M., & Cervera, M. A. (2004). Buckland Park all-sky interferometric meteor radar. *Radio Science*, *39*(5). https://doi.org/10.1029/2003RS003014

Hong, S.-S., & Lindzen, R. S. (1976). Solar Semidiurnal Tide in the Thermosphere. *Journal of the Atmospheric Sciences*, *33*(1), 135–153. https://doi.org/10.1175/1520-0469(1976)033⟨0135:SSTITT⟩2.0.CO;2

Jacobi, C. (2012). 6 year mean prevailing winds and tides measured by VHF meteor radar over Collm (51.3N, 13.0E). *Journal of Atmospheric and Solar-Terrestrial Physics*, *78–79*, 8–18. https://doi.org/10.1016/j.jastp.2011.04.010

Jacobi, C., Fröhlich, K., Portnyagin, Y., Merzlyakov, E., Solovjova, T., Makarov, N., et al. (2009). Semi-empirical model of middle atmosphere wind from the ground to the lower thermosphere. *Advances in Space Research*, *43*(2), 239–246. https://doi.org/10.1016/j.asr.2008.05.011

Jin, H., Miyoshi, Y., Pancheva, D., Mukhtarov, P., Fujiwara, H., & Shinagawa, H. (2012). Response of migrating tides to the stratospheric sudden warming in 2009 and their effects on the ionosphere studied by a whole atmosphere-ionosphere model GAIA with COSMIC and TIMED/SABER observations. *Journal of Geophysical Research*, *117*(A10). https://doi.org/10.1029/2012JA017650

Jones, M., Jr., Forbes, J. M., Hagan, M. E., & Maute, A. (2014). Impacts of vertically propagating tides on the mean state of the ionosphere-thermosphere system. *Journal of Geophysical Research: Space Physics*, *119*, 2197–2213. https://doi.org/10.1002/2013JA019744

Körnich, H., & Becker, E. (2010). A simple model for the interhemispheric coupling of the middle atmosphere circulation. *Advances in Space Research*, *45*(5), 661–668. https://doi.org/10.1016/j.asr.2009.11.001

Lieberman, R. S., Riggin, D. M., Franke, S. J., Manson, A. H., Meek, C., Nakamura, T., et al. (2003). The 6.5-day wave in the mesosphere and lower thermosphere: Evidence for baroclinic/barotropic instability. *Journal of Geophysical Research*, *108*(D20). https://doi.org/10.1029/2002JD003349

Lieberman, R. S., Riggin, D. M., Ortland, D. A., Nesbitt, S. W., & Vincent, R. A. (2007). Variability of mesospheric diurnal tides and tropospheric diurnal heating during 1997–1998. *Journal of Geophysical Research*, *112*(D20). https://doi.org/10.1029/2007JD008578

Lindzen, R. S., & Hong, S.-s (1974). Effects of mean winds and horizontal temperature gradients on solar and lunar semidiurnal tides in the atmosphere. *Journal of the Atmospheric Sciences*, *31*(5), 1421–1446. https://doi.org/10.1175/1520-0469(1974)031⟨1421:EOMWAH⟩2.0.CO;2

Liu, H.-L., Bardeen, C. G., Foster, B. T., Lauritzen, P., Liu, J., Lu, G., et al. (2018). Development and validation of the whole atmosphere community climate model with thermosphere and ionosphere extension (WACCM-X 2.0). *Journal of Advances in Modeling Earth Systems*, *10*(2), 381–402. https://doi.org/10.1002/2017MS001232

Liu, H.-L., & Hagan, M. E. (1998). Local heating/cooling of the mesosphere due to gravity wave and tidal coupling. *Geophysical Research Letters*, *25*(15), 2941–2944. https://doi.org/10.1029/98GL02153

Liu, H.-L., Li, T., She, C.-Y., Oberheide, J., Wu, Q., Hagan, M. E., et al. (2007). Comparative study of short-term diurnal tidal variability. *Journal of Geophysical Research*, *112*(D18). https://doi.org/10.1029/2007JD008542

Liu, H.-L., & Richmond, A. D. (2013). Attribution of ionospheric vertical plasma drift perturbations to large-scale waves and the dependence on solar activity. *Journal of Geophysical Research: Space Physics*, *118*, 2452–2465. https://doi.org/10.1002/jgra.50265

Liu, H.-L., Roble, R. G., Taylor, M. J., & Pendleton, W. R., Jr. (2001). Mesospheric planetary waves at northern hemisphere fall equinox. *Geophysical Research Letters*, *28*(9), 1903–1906. https://doi.org/10.1029/2000GL012689

Liu, H.-L., Talaat, E. R., Roble, R. G., Lieberman, R. S., Riggin, D. M., & Yee, J.-H. (2004). The 6.5-day wave and its seasonal variability in the middle and upper atmosphere. *Journal of Geophysical Research*, *109*(D21). https://doi.org/10.1029/2004JD004795

Liu, J., Liu, H., Wang, W., Burns, A. G., Wu, Q., Gan, Q., et al. (2018). First results from the ionospheric extension of WACCM-X during the deep solar minimum year of 2008. *Journal of Geophysical Research: Space Physics*, *123*, 1534–1553. https://doi.org/10.1002/2017JA025010

Marsh, D. R., Mills, M. J., Kinnison, D. E., Lamarque, J. F., Calvo, N., & Polvani, L. M. (2013). Climate change from 1850 to 2005 simulated in CESM1(WACCM). *Journal of Climate*, *26*, 7372–7391. https://doi.org/10.1175/JCLI-D-12-00558.1

McLandress, C., Jonsson, A. I., Plummer, D. A., Reader, M. C., Scinocca, J. F., & Shepherd, T. G. (2010). Separating the dynamical effects of climate change and ozone depletion. Part I: Southern Hemisphere stratosphere. *Journal of Climate*, *23*(18), 5002–5020. https://doi.org/10.1175/2010JCLI3586.1

Millward, G. H., Müller-Wodarg, I. C. F., Aylward, A. D., Fuller-Rowell, T. J., Richmond, A. D., & Moffett, R. J. (2001). An investigation into the influence of tidal forcing on F region equatorial vertical ion drift using a global ionosphere-thermosphere model with coupled electrodynamics. *Journal of Geophysical Research: Space Physics*, *106*(A11), 24733–24744. https://doi.org/10.1029/2000JA000342

Miyahara, S., & Wu, D.-H. (1989). Effects of solar tides on the zonal mean circulation in the lower thermosphere: solstice condition. *Journal of Atmospheric and Terrestrial Physics*, *51*(7), 635–647. https://doi.org/10.1016/0021-9169(89)90062-7

Neale, R. B., Richter, J., Park, S., Lauritzen, P. H., Vavrus, S. J., Rasch, P. J., & Zhang, M. (2013). The mean climate of the Community Atmosphere Model (CAM4) in forced SST and fully coupled experiments. *Journal of Climate*, *26*, 5150–5168. https://doi.org/10.1175/JCLI-D-12-00236.1

Palo, S. E., Forbes, J. M., Zhang, X., Russell, J. M., III, & Mlynczak, M. G. (2007). An eastward propagating two-day wave: Evidence for nonlinear planetary wave and tidal coupling in the mesosphere and lower thermosphere. *Geophysical Research Letters*, *34*. https://doi.org/10.1029/2006GL027728

Pedatella, N. M., Richmond, A. D., Maute, A., & Liu, H.-L. (2016). Impact of semidiurnal tidal variability during SSWs on the mean state of the ionosphere and thermosphere. *Journal of Geophysical Research: Space Physics*, *121*, 8077–8088. https://doi.org/10.1002/2016JA022910

Sandford, D. J., Muller, H. G., & Mitchell, N. J. (2006). Observations of lunar tides in the mesosphere and lower thermosphere at Arctic and middle latitudes. *Atmospheric Chemistry and Physics*, *6*(12), 4117–4127. https://doi.org/10.5194/acp-6-4117-2006

Senf, F., & Achatz, U. (2011). On the impact of middle-atmosphere thermal tides on the propagation and dissipation of gravity waves. *Journal of Geophysical Research*, *116*(D24). https://doi.org/10.1029/2011JD015794

Siddiqui, T. A., Maute, A., & Pedatella, N. M. (2019). On the importance of interactive ozone chemistry in earth-system models for studying mesophere-lower thermosphere tidal changes during sudden stratospheric warmings. *Journal of Geophysical Research: Space Physics*, *124*, 10690–10707. https://doi.org/10.1029/2019JA027193

Smith, A. K., Garcia, R. R., Marsh, D. R., Kinnison, D. E., & Richter, J. H. (2010). Simulations of the response of mesospheric circulation and temperature to the Antarctic ozone hole. *Geophysical Research Letters*, *37*(22). https://doi.org/10.1029/2010GL045255

Smith, A. K., Pedatella, N. M., Marsh, D. R., & Matsuo, T. (2017). On the dynamical control of the mesosphere–lower thermosphere by the lower and middle atmosphere. *Journal of the Atmospheric Sciences*, *74*(3), 933–947. https://doi.org/10.1175/JAS-D-16-0226.1

Smith, A. K., Pedatella, N. M., & Mullen, Z. K. (2020). Interhemispheric coupling mechanisms in the middle atmosphere of WACCM6. *Journal of the Atmospheric Sciences*, *77*(3), 1101–1118. https://doi.org/10.1175/JAS-D-19-0253.1

Stening, R. J., Forbes, J. M., Hagan, M. E., & Richmond, A. D. (1997). Experiments with a lunar atmospheric tidal model. *Journal of Geophysical Research*, *102*(D12), 13465–13471. https://doi.org/10.1029/97JD00778

Swinbank, R., & Ortland, D. A. (2003). Compilation of wind data for the Upper Atmosphere Research Satellite (UARS) reference atmosphere project. *Journal of Geophysical Research*, *108*(D19). https://doi.org/10.1029/2002JD003135

Talaat, E. R., Yee, J.-H., & Zhu, X. (2001). Observations of the 6.5-day wave in the mesosphere and lower thermosphere. *Journal of Geophysical Research*, *106*(D18), 20715–20723. https://doi.org/10.1029/2001JD900227

Taylor, M. J., Pendleton, W. R., Jr., Liu, H.-L., She, C. Y., Gardner, L. C., Roble, R. G., & Vasoli, V. (2001). Large amplitude perturbations in mesospheric OH Meinel and 87-Km Na lidar temperatures around the autumnal equinox. *Geophysical Research Letters*, *28*(9), 1899–1902. https://doi.org/10.1029/2000GL012682

Teitelbaum, H., & Vial, F. (1991). On tidal variability induced by nonlinear interaction with planetary waves. *Journal of Geophysical Research*, *96*(A8), 14169–14178. https://doi.org/10.1029/91JA01019

Venkateswara Rao, N., Espy, P. J., Hibbins, R. E., Fritts, D. C., & Kavanagh, A. J. (2015). Observational evidence of the influence of Antarctic stratospheric ozone variability on middle atmosphere dynamics. *Geophysical Research Letters*, *42*(19), 7853–7859. https://doi.org/10.1002/2015GL065432

Warner, K., & Oberheide, J. (2014). Nonmigrating tidal heating and MLT tidal wind variability due to the El Niño–Southern Oscillation. *Journal of Geophysical Research: Atmospheres*, *119*, 1249–1265. https://doi.org/10.1002/2013JD020407

Waugh, D. W., & Randel, W. J. (1999). Climatology of Arctic and Antarctic polar vortices using elliptical diagnostics. *Journal of the Atmospheric Sciences*, *56*(11), 1594–1613. https://doi.org/10.1175/1520-0469(1999)056<1594:COAAAP>2.0.CO;2

Waugh, D. W., Randel, W. J., Pawson, S., Newman, P. A., & Nash, E. R. (1999). Persistence of the lower stratospheric polar vortices. *Journal of Geophysical Research*, *104*(D22), 27191–27201. https://doi.org/10.1029/1999JD900795

Yamazaki, Y., & Richmond, A. D. (2013). A theory of ionospheric response to upward-propagating tides: Electrodynamic effects and tidal mixing effects. *Journal of Geophysical Research: Space Physics*, *118*, 5891–5905. https://doi.org/10.1002/jgra.50487